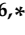


Article

A Thermal Sublimation Generator of ^{131m}Xe

Karolina Kulesz^{1,2}, Nikolay Azaryan¹, Mikołaj Baranowski³, Mateusz Jerzy Chojnacki^{1,2}, Ulli Köster⁴, Razvan Lica^{1,5}, Sorin Gabriel Pascu^{1,5}, Renaud Blaise Jolivet^{6,*} and Magdalena Kowalska^{1,*}

¹ CERN, Espl. des Particules 1, 1211 Meyrin, Switzerland

² Faculty of Science, University of Geneva, Quai Ernest-Ansermet 24, 1211 Geneva, Switzerland

³ Faculty of Physics, Adam Mickiewicz University, Umultowska 85, 61-614 Poznan, Poland

⁴ Institut Laue-Langevin (ILL), 71 Avenue des Martyrs, 38000 Grenoble, France

⁵ Horia Hulubei National Institute of Physics and Nuclear Engineering (IFIN-HH), Reactorului 30 St., 077125 Bucharest-Magurele, Romania

⁶ Maastricht Centre for Systems Biology (MaCSBio), Maastricht University, Paul-Henri Spaaklaan 1, 6229 EN Maastricht, The Netherlands

* Correspondence: rjolivet@maastrichtuniversity.nl (R.B.J.); Magdalena.Kowalska@cern.ch (M.K.)

Abstract: Stable and unstable isotopes of the heavy noble gas xenon find use in various medical applications. However, apart from ^{133}Xe , used for Single Photon Emission Computed Tomography, radioactive isotopes of xenon are currently complicated to obtain in small quantities. With the GAMMA-MRI project in mind, we investigated a thermal sublimation generator of the long-lived excited state (isomer) ^{131m}Xe . This production method utilized the decay of ^{131}I , obtained commercially from a hospital supplier in the form of Na^{131}I powder. Heat treatments of the Na^{131}I powder and cryogenic trapping of released ^{131m}Xe allowed us to collect up to 88% of the produced xenon. Our method provides an isomeric mixture of ^{131m}Xe and ^{131}Xe . With improvements in scalability and chemical purification, this method could be a cost-effective source of ^{131m}Xe for small-scale experiments.

Keywords: radioisotopes production; xenon production; ^{131m}Xe ; ^{131}I radioactive decay; Na^{131}I



Citation: Kulesz, K.; Azaryan, N.; Baranowski, M.; Chojnacki, M.J.; Köster, U.; Lica, R.; Pascu, S.G.; Jolivet, R.B.; Kowalska, M. A Thermal Sublimation Generator of ^{131m}Xe . *Instruments* **2022**, *6*, 76. <https://doi.org/10.3390/instruments6040076>

Academic Editor: Ivor Fleck

Received: 17 September 2022

Accepted: 7 November 2022

Published: 16 November 2022

Publisher's Note: MDPI stays neutral with regard to jurisdictional claims in published maps and institutional affiliations.



Copyright: © 2022 by the authors. Licensee MDPI, Basel, Switzerland. This article is an open access article distributed under the terms and conditions of the Creative Commons Attribution (CC BY) license (<https://creativecommons.org/licenses/by/4.0/>).

1. Introduction

Stable and radioactive isotopes of xenon are used in large quantities in medical imaging and Nuclear Magnetic Resonance (NMR) applications [1–5]. Xenon has several important qualities [1]. First, it is inert, and does not interact chemically with the research subject, or sample [1]. Second, the amplitude of the NMR signal acquired from xenon can be increased by several orders of magnitude if xenon is hyperpolarized by colliding it with optically pumped alkali atoms using Spin Exchange Optical Pumping (SEOP) [6]. In addition, xenon passively crosses the blood brain barrier, and can serve as a contrast agent to image the uptake of the inhaled gas into brain tissue. This can be used effectively for stroke diagnosis for instance [7]. The most widely used stable isotopes of xenon are the nuclear ground states of ^{129}Xe and ^{131}Xe . They are typically used in NMR studies of materials, and for Magnetic Resonance Imaging (MRI) of the lungs [8–11]. Unstable ^{133}Xe is used in Single Photon Emission Computed Tomography (SPECT) for the diagnosis of pulmonary diseases [12,13]. The physical half-life of ^{133}Xe (5.3 d) makes it easy for radiopharmaceutical suppliers to manufacture and deliver it [13].

In the GAMMA-MRI project [14], we aim at developing a new imaging technique based on the MRI response from polarized unstable, SPECT-compatible nuclei. Our first test cases are radioactive xenon isomers, in particular the long-lived ^{129m}Xe , ^{131m}Xe , and ^{133m}Xe isomers. Optimising SEOP polarization of these isomers is one of the key components of the GAMMA-MRI project. For this purpose, it is advantageous to use the isomer that has the longest half-life, and that can be produced in an affordable way.

Here, we explore a generator of ^{131m}Xe ($t_{1/2} = 11.84$ d), via decay of a ^{131}I source ($t_{1/2} = 8.02$ d) obtained commercially from a hospital supplier. ^{131}I , like ^{133}Xe in its ground

state, is in high demand by hospitals and thus can be procured from radiopharmaceutical companies [15,16]. Both ^{131}I and ^{133}Xe can be produced from ^{235}U fission, upon ^{235}U irradiation with neutrons in nuclear reactor facilities: $^{235}\text{U}(n, f)^{133}\text{Xe}$ and $^{235}\text{U}(n, f)^{131}\text{I}$ [17]. To isolate and collect these isotopes, the ^{235}U target is dissolved, and the solution is separated into cells containing specific chemically active elements [18]. This approach offers several benefits: a flexible delivery schedule (medical ^{131}I is available > 350 d/yr), established supply routes (to hospitals), and a relatively low cost for samples at the delivery point.

$^{131\text{m}}\text{Xe}$ generators based on ^{131}I have been investigated before. For instance, P. Bedrossian [19] used a palladium metal surface to adsorb ^{131}I from a solution. That generator was then connected to a vacuum-tight setup placed vertically: with generator atop and a set of glass spheres underneath. Produced $^{131\text{m}}\text{Xe}$ was collected in the bottom-most glass sphere immersed in the liquefied air, and the sphere was separated by sealing it off with a flame torch. In [20], a $^{131\text{m}}\text{Xe}$ generator is described, where a ^{131}I solution was precipitated onto a fibreglass filter as palladium(II) iodide PdI_2 , inside a commercially available syringe filter. The syringe was connected to a carrier gas which, after the desired quantity of $^{131\text{m}}\text{Xe}$ was produced, would sweep the $^{131\text{m}}\text{Xe}$ from the syringe filter into another apparatus for γ -ray spectroscopy. Both of these generators reported near unity $^{131\text{m}}\text{Xe}$ production efficiency. Finally, in a more recent publication [21], the production of $^{131\text{m}}\text{Xe}$ from ^{131}I is mentioned but no details are given. However, to the best of our knowledge, $^{131\text{m}}\text{Xe}$ production from Na^{131}I powder has not been reported yet.

Here, we fill this gap and report on $^{131\text{m}}\text{Xe}$ production from a Na^{131}I powder. A solid state sample is preferred for the GAMMA-MRI project. Specifically, it should introduce less water into the SEOP cell than a Na^{131}I solution. It is important for successful polarization to eliminate all sources of water that could oxidize rubidium used in the SEOP process. The objective of the present work was thus to establish the most suitable conditions to extract $^{131\text{m}}\text{Xe}$ from a Na^{131}I salt, and to optimize the collection efficiency.

2. Materials and Methods

Production of $^{131\text{m}}\text{Xe}$ from ^{131}I decay involved the following procedure: (i) procurement of the ^{131}I source in the form of powder encapsulated in a gelatin shell, (ii) γ -ray spectroscopy of the ^{131}I source upon arrival at CERN, (iii) Na^{131}I powder transfer from its gelatin shell in a quartz tube and γ -ray spectroscopy of both constituents, (iv) placement of the powder in the experimental installation for decay, (v) collection of $^{131\text{m}}\text{Xe}$ from the Na^{131}I powder at ambient temperature, or after heating, and finally (vi) $^{131\text{m}}\text{Xe}$ γ -ray spectroscopy. Three 50(5) MBq Na^{131}I samples were purchased from Curium Pharma (Curium Pharma, Paris, France)—a supplier who could regularly deliver a Na^{131}I source at high radionuclidic purity (see Section 2.2). The samples were processed according to the procedure described above.

2.1. Characteristics of the Parent Source

The parent nucleus for the $^{131\text{m}}\text{Xe}$ generator is ^{131}I . The following characteristics were considered: the half-life $t_{1/2}$ and the branching ratio BR_m for the transition to $^{131\text{m}}\text{Xe}$, the isotopic and chemical purity of ^{131}I , the state of ^{131}I (solid or liquid), its availability, the associated radiological risks, and finally the cost of the ^{131}I source and of its delivery.

^{131}I ($t_{1/2} = 8.02$ d) is a beta-gamma (β^- , γ) ray emitter, which decays to the isomer $^{131\text{m}}\text{Xe}$ ($t_{1/2} = 11.84$ d), and to the ground state ^{131}Xe (stable). While the dominant part of β^- decays of ^{131}I feeds the ground state $^{131\text{g}}\text{Xe}$, a small fraction of $BR_m = 1.09(9)\%$ feeds the isomer $^{131\text{m}}\text{Xe}$ [22].

The amount of collected $^{131\text{m}}\text{Xe}$ nuclei is, thus, the result of two competing processes, a source term from the decay of ^{131}I , and a sink term due to $^{131\text{m}}\text{Xe}$ decay. The mathematical model describing isotopes in the decay chain ($^{131}\text{I} > ^{131\text{m}}\text{Xe} > ^{131}\text{Xe}$) as a function of time is Bateman's equation [23], which for ^{131}I gives:

$$A_{\text{mXe}}(t) = \lambda_{\text{mXe}} N_{\text{mXe}}(t) = BR_m N_{\text{I}0} \frac{\lambda_{\text{I}} \lambda_{\text{mXe}}}{\lambda_{\text{mXe}} - \lambda_{\text{I}}} (e^{-\lambda_{\text{I}} t} - e^{-\lambda_{\text{mXe}} t}) + \lambda_{\text{mXe}} N_{\text{mXe}}(0) e^{-\lambda_{\text{mXe}} t}, \quad (1)$$

with $A_{mXe}(t)$ activity of ^{131m}Xe at time t , N_{I_0} the number of ^{131}I nuclei at $t_0 = 0$, decaying into $N_{mXe}(t)$ ^{131m}Xe nuclei at the rate λ_I in time t and with the branching ratio BR_m . Additionally, ^{131m}Xe decays into stable ^{131}Xe at the rate λ_{mXe} in time t . The second term $\lambda_{mXe}N_{mXe}(0)e^{-\lambda_{mXe}t}$ describes the decay of ^{131m}Xe present in the system at moment $t_0 = 0$.

Figure 1 illustrates Equation (1) assuming $N_{mXe}(0) = 0$ and the initial activity of ^{131}I $A_I(0) = 1$ MBq. The figure presents the activity in function of time: the decay of ^{131}I (activity in black, uncertainty in grey) in MBq, and the production and decay of ^{131m}Xe (activity in red, uncertainty in yellow) in kBq. The error bars comprise the errors of the decay constant and branching ratio. The optimum waiting time, when the daughter activity is maximal, can be calculated analytically by finding the maximum t_{opt} of function in Equation (1). After transformation, the equation reads:

$$t_{opt} = \frac{\ln \frac{\lambda_I}{\lambda_{mXe}}}{\lambda_I - \lambda_{mXe}} \quad (2)$$

and $t_{opt} = 14.0$ days. The maximum ^{131m}Xe activity is 3.23(1) kBq and it corresponds to 0.324(1)% of the initial activity of the ^{131}I source placed in the experimental setup.

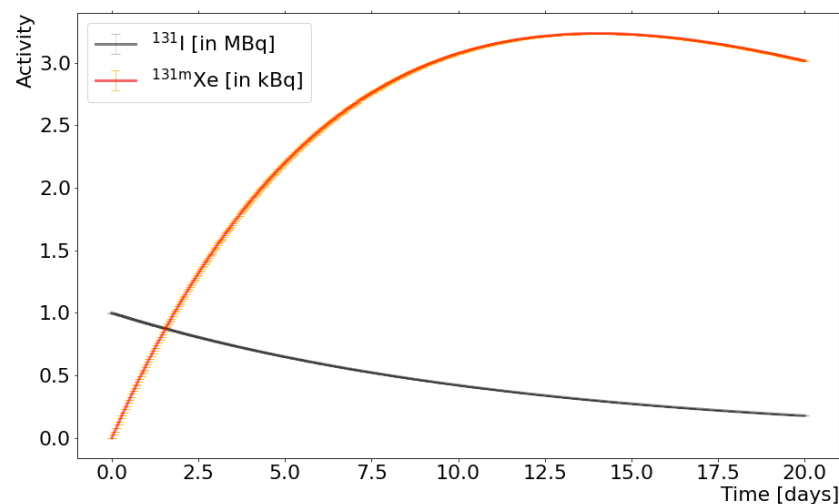


Figure 1. Calculated ^{131m}Xe activity (red) vs. time. A source of ^{131}I (activity in black, uncertainty in grey) decays into ^{131m}Xe (activity in red, uncertainty in yellow), which itself decays into ^{131}Xe (stable, not shown). The error bars comprise the errors of the decay constant and branching ratio. The maximum activity plateau for ^{131m}Xe is at day 14 (Equation (2)).

2.2. ^{131}I Source Manufacturing

Radiopharmaceutical preparation standards are defined in European Pharmacopoeia [24], and implemented by all manufacturers in Europe. They define the quality of ^{131}I medication, including the chemical and radionuclidic purity, and define accepted physical forms and dosage. The radionuclidic purity of ^{131}I is $\geq 99.9\%$ with ^{133}I , ^{135}I and other impurities $\leq 0.01\%$.

The ^{131}I bulk solution is delivered on a regular basis to our supplier Curium Pharma by the processors of reactor-irradiated targets, which extract the ^{131}I from targets. The solution already includes excipients, added to prevent the escape of significant amounts of dissolved volatile iodine [25]. In addition, those excipients are necessary to adjust the pH of the ^{131}I bulk solution, and to flavour the medicine for patients. For our application however, the additional ingredients can indirectly affect the purity of the collected ^{131m}Xe , as detailed in Section 3.

Curium Pharma provides ^{131}I directly to hospitals and other partners (e.g., CERN) in a liquid NaI solution (shipped in a glass vial), or in the solid state (NaI powder in a gelatin capsule). Na ^{131}I in the capsule format used in this work is prepared by adding a small volume of the solution to a NaI powder placed in a gelatin shell. Figure 2 shows one such capsule and the powder, in scale.

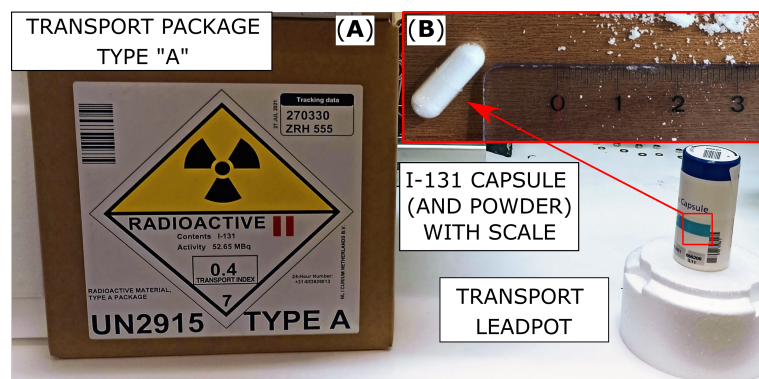


Figure 2. Standard elements of the transport packaging of the radiopharmaceutical ^{131}I . (A) Type-A package. The lead container, held securely in polystyrene foam inside a cardboard box. (B) Gelatin capsule and Na^{131}I powder.

2.3. Purchase of ^{131}I and Radioactive Decay

For every experiment, a single capsule containing Na^{131}I was delivered to CERN in a lead pot in a type-A package (Figure 2). The manufacturer specifies the activity to 10%, i.e., 50(5) MBq. Upon arrival, the actual ^{131}I activity in the capsule was determined with a n-type calibrated Extended Range (XtRa) Coaxial Ge detector (model GX6020, Canberra, Montigny-Le-Brettonneux, France) with a thin carbon window. As an acquisition system, we used a multichannel analyzer model ASPEC-927 and Maestro-32 software (AMETEK ORTEC, Oak Ridge, TN, USA). Remote manipulators with machined grooves were used to open the gelatin shell, and to transport its content into a dedicated borosilicate glass tube. Figure 3 presents the tools used for the safe handling of the capsule. These were necessary to avoid exposure to a large radiation dose received directly to the operator's fingers.

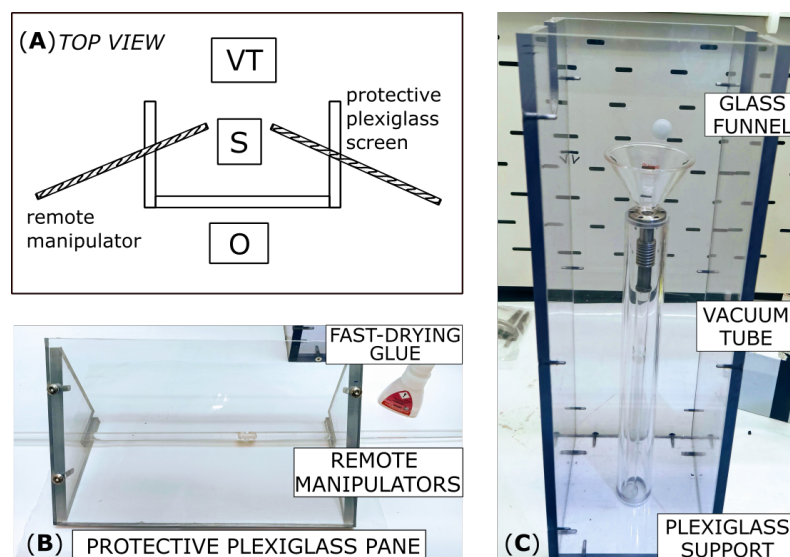


Figure 3. (A) Schematic of the opening setup. Operator (O) stands behind the protective panel and manipulates the source (S) with remote manipulators. The source is transferred to a glass tube that is then installed in the vacuum-tight experimental setup (labelled vacuum tube or VT in the schematic). (B) The tools for safe handling of the source included: the acrylic remote manipulators with grooves machined to the size of the gelatin shell, the acrylic shielding panel (thickness 1 cm) stopping beta particles from the ^{131}I source, and the fast-drying glue necessary for the rapid attachment of the gelatin shell to the grooves in the acrylic manipulators. (C) The acrylic support for the vacuum tube: a borosilicate glass annealing tube with a CF 16 flange. A glass funnel aids powder transfer and minimizes transfer losses.

Using the acrylic manipulators with a drop of fast drying glue UHU solvent-free Flex Tube to attach the gelatin shell, the capsule was open into two halves. With the acrylic manipulators, the Na^{131}I powder was then transferred from the gelatin capsule via a glass funnel into the borosilicate glass annealing tube (labelled VT or vacuum tube in Figure 3). γ -ray spectroscopy on the annealing vial containing the powder provided a measurement of the activity of the transferred powder, and of the potential losses due to capsule manipulations, as detailed in Section 3.1. Next, the tube was installed in the experimental setup for xenon production.

2.4. ^{131}I Extraction and $^{131\text{m}}\text{Xe}$ Collection

The setup for $^{131\text{m}}\text{Xe}$ collection (Figure 4) consisted of ultrahigh vacuum (UHV) elements (CF flanges, needle valves and gate valves). In addition, the setup contained the annealing tube with Na^{131}I and a collection vial for $^{131\text{m}}\text{Xe}$, both made of borosilicate glass.

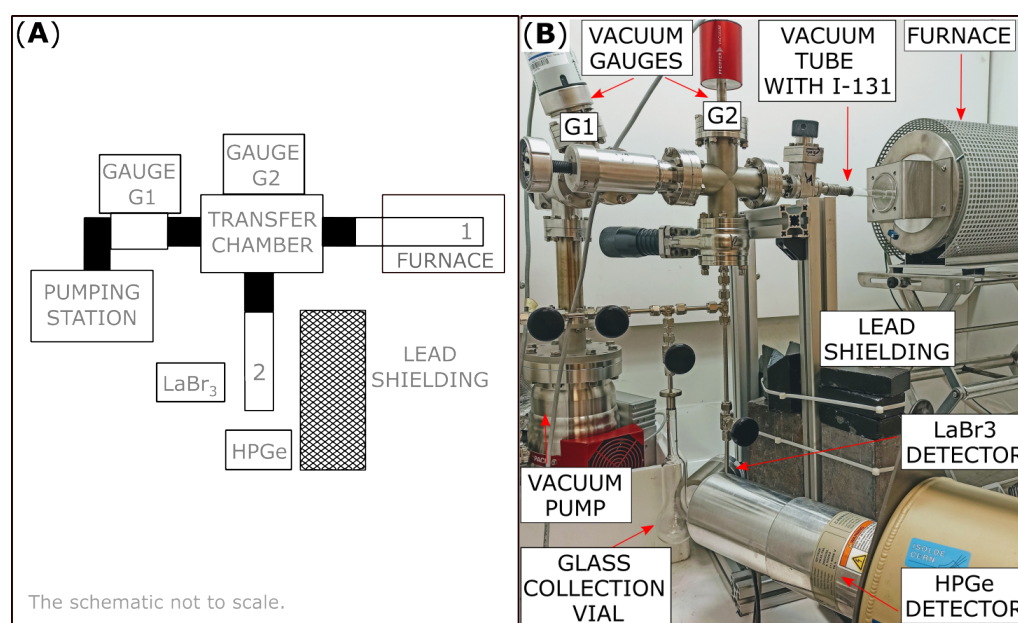


Figure 4. (A) A schematic of the extraction setup. The Na^{131}I source (labelled 1) is in the glass annealing tube inside the furnace. The collection vial for $^{131\text{m}}\text{Xe}$ is labelled 2. Black rectangles denote valves dividing the installation into separate cells. The full-range vacuum gauge (labelled G1) was mounted at the interface between the pumping station and the transfer chamber. The capacitance diaphragm vacuum gauge (labelled G2) was mounted to the transfer chamber (B) A photograph of the experimental installation for xenon extraction and collection.

An UHV valve was mounted between the annealing tube and rest of the setup. The tip of the tube which contained the transferred Na^{131}I powder was inserted into a furnace equipped with temperature stability controls (measured temperature drift ≤ 2 °K). The Na^{131}I powder was heated to up to 400 °C to allow for xenon to diffuse out of the powder. Each heating treatment lasted one hour, with increasing temperatures for consecutive treatments. The collection vial was mounted vertically in the setup. The free space below it was used to place a container with liquid nitrogen—a cryotrap—for $^{131\text{m}}\text{Xe}$ collection. Collections were performed after every one-hour-long heat treatment.

The experimental setup was evacuated to 10^{-6} mbar with a turbomolecular pump, and an oil-free scroll pump. Two pressure gauges were integrated into the system to cover the pressure range from UHV to atmospheric pressure. A full-range vacuum gauge (labelled G1 in Figure 4) housing two sensors—a Pirani gauge and a cold-cathode ionization gauge—was installed between the pumping system and the chamber in contact with xenon. This location was optimal for a wide range of vacuum regimes, but it was not used in the presence of xenon, due to the ionic pumping effect. A capacitance diaphragm vacuum gauge (labelled G2 in Figure 4) was installed at the interface between the gas diffusing from the annealing vial

and the collection vial. That gauge measured the direct force on the diaphragm, and could consequently measure the pressure independently of gas type and concentration. In addition, it did not pump xenon like an ionization gauge would.

After each collection, the valve to the collection vial was closed and the cryotrap was removed to allow in situ γ -ray spectroscopy to characterize how collections depended on the temperature of the heating cycles. We used two γ -ray detectors. The first one was a 2×2 inch LaBr₃(Ce) crystal encapsulated in aluminium. Thin aluminium housing and a glass light guide allowed for acquisition of 29.8 keV X-rays from decay of ^{131m}Xe to the ground state (branching ratio 29.3%). The latter was a n-type Standard Electrode Coaxial Ge (SEGe) detector, model GC7020 (Canberra), with an aluminium window blocking X-ray radiation (including at 29.3 keV), but sensitive to higher energy radiation (^{131m}Xe: 163.9 keV and ¹³¹I: 364.5 keV). We used the CAEN DT5730 (8 Channel 14 bit 500 MS/s Digitizer) with the PHA firmware and Compass software [26]. The distance between the center axis of the collection vial and the detectors was 55 mm and 80 mm, respectively, for the LaBr₃(Ce) and the HPGe detector. A 10-cm-thick lead shielding was placed between the Na¹³¹I source and the detectors to reduce the ¹³¹I background, and to prevent saturating the HPGe preamplifier due to high count rates from the iodine source. The Na¹³¹I source was at the distance of about 60 cm from the detectors.

After completion of the heat treatment cycles, the collection vial with xenon was detached from the experimental setup, and transported to a second γ -ray spectroscopy station, with the Canberra n-type XtRa Ge detector, model GX6020, for a posteriori precise determination of activity, without the ¹³¹I background (as detailed in Section 3.1). The sources of ¹⁵²Eu and ¹³³Ba with known absolute activities were used for the energy calibration and for the determination of the absolute detection efficiency at energies $E_\gamma < 1.5$ MeV. These calibrated sources were measured at the source-detector distance d equal 50 cm (used for γ -ray spectroscopy of ^{131m}Xe collection vial) and 154 cm (used for γ -ray spectroscopy of high-activity Na¹³¹I powder). See Figure 5 for the absolute efficiency plotted in function of the energy for $d = 50$ cm.

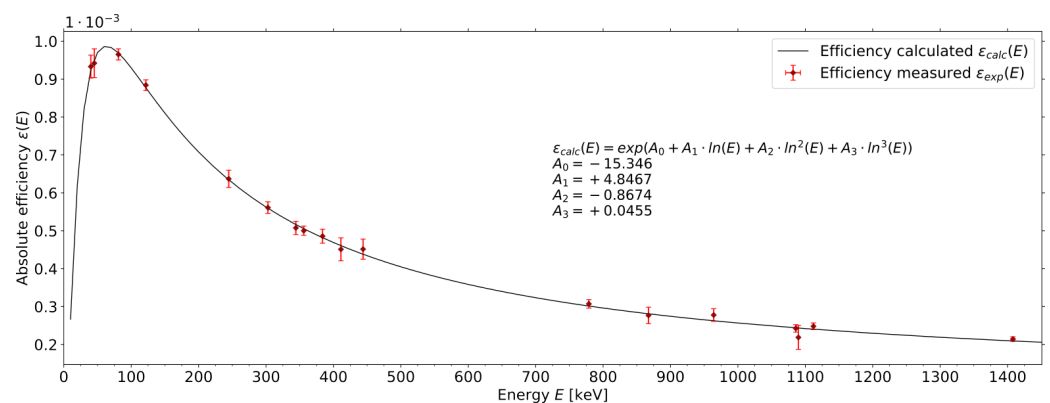


Figure 5. Absolute efficiency for n-type Extended Range Coaxial Ge detector (XtRa), model GX6020 at the distance of 50 cm from the source. Measured efficiency $\varepsilon_{exp}(E)$ (in red) was plotted based on ¹⁵²Eu and ¹³³Ba measurements. A polynomial of 3rd degree $\varepsilon_{calc}(E)$ (in black) was fitted to the experimental data. The equation and fit parameters are enclosed in Figure.

The coefficient of determination R^2 for the fitted 3rd degree polynomial was 0.996. The absolute efficiency curve in Figure 5 presents a well-known knee around 100 keV. This effect was accounted for by fitting to the dataset that included 4 γ rays in the 40–130 keV energy range. The accuracy determined as $a(E) = \frac{\varepsilon_{exp}(E) - \varepsilon_{calc}(E)}{\varepsilon_{exp}(E)} \cdot 100$ was calculated for the energy range near γ radiation characteristic for ^{131m}Xe (163.9 keV) and ¹³¹I (364.5 keV). That accuracy for selected ¹⁵²Eu and ¹³³Ba γ -ray peaks equaled $a(81.0) = 0.39\%$, $a(121.8) = 0.78\%$, $a(244.7) = 0.38\%$, and $a(356.0) = 1.09\%$. It confirmed good accuracy of the fit in the energy region characteristic for γ -radiation from ¹³¹I and

^{131m}Xe decay. The absolute efficiencies for 163.9 keV from ^{131m}Xe and for 364.5 keV ^{131}I were listed in Table 1.

Table 1. Absolute efficiencies for 163.9 keV and 364.5 keV (Canberra XtRa detector, model GX6020).

Source	Distance d : Source–Detector [cm]	Energy [keV]	Detection Efficiency
^{131m}Xe vial	50	163.9	$7.79(15)\cdot 10^{-4}$
		364.5	$4.98(12)\cdot 10^{-4}$
Na^{131}I powder	154	364.5	$5.65(13)\cdot 10^{-5}$

In activity calculations, transmission through glass and air were taken into account. Attenuation of 364.5 keV γ -ray in the Na^{131}I powder was neglected due to the high porosity of the powder and inhomogeneous spread of ^{131}I onto NaI matrix (from the drop casting technique used for bulk ^{131}I solution). This attenuation coefficient was determined to be, at most 2% given the NaI grain size of 0.4 mm radius (path of X-ray).

3. Results

3.1. Efficiency of ^{131m}Xe Generator

Three types of γ -ray spectroscopy measurements (see Section 2) were taken and used for the calculations of: activity of the Na^{131}I capsule, activity of the Na^{131}I powder transferred to the vial, and activity of the collected ^{131m}Xe . Analyzed spectra consisted of background counts and counts in the area of interest. To derive the activity of samples, the number of counts in the peak areas was calculated using ORTEC-MAESTRO Multi-channel Analyzer [27]. Linear background subtraction and Gaussian fitting were applied in regions of interest (ROIs).

A typical spectrum is shown in Figure 6 for the transferred ^{131}I powder and in Figure 7 for the collected ^{131m}Xe . In Figure 6, the main γ -ray transitions for ^{131}I are marked and labelled: 364.5 keV (branching ratio 81.5%), 637.0 keV (7.16%), 284.3 keV (6.12%), 80.2 keV (2.6%), and 722.9 keV (1.8%) [22]. The γ -ray decay branch at 364.5 keV was used for the determination of the ^{131}I activity. The sample was also verified for presence of impurities (mostly ^{133}I and ^{135}I), and no impurities were found.

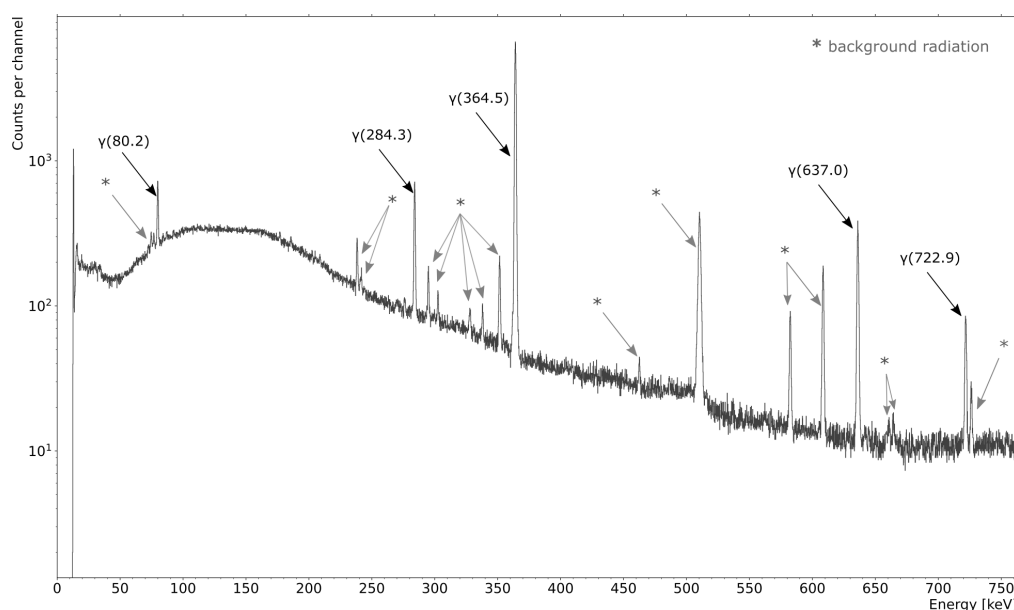


Figure 6. γ -ray spectroscopy of the ^{131}I powder after the transfer into the annealing vial, recorded in the ISOLDE experimental hall. The γ radiation characteristic of ^{131}I is labelled in black. These are lines at: 364.5 keV (81.5%), 637.0 keV (7.16%), 284.3 keV (6.12%), 80.2 keV (2.6%), and 722.9 keV (1.8%). The background γ radiation is marked with grey stars in the plot.

The γ -ray lines marked grey and starred in Figures 6 and 7 belong to the natural background gamma-radiation: ^{137}Cs (661.66 keV), ^{208}Tl (277.4 keV, 510.8 keV, 583.2 keV), ^{212}Bi (727.3 keV), ^{212}Pb (238.6 keV, 300.1 keV), ^{214}Bi (609.3 keV, 665.5 keV), ^{214}Pb (74.8 keV, 77.1 keV, 242.0 keV, 295.2 keV, 351.9 keV), ^{228}Ac (209.3 keV, 270.2 keV, 327.5 keV, 328.0 keV, 338.3 keV, 463.0 keV, 509.0 keV, 726.9 keV), and electron–positron annihilation peak at 511 keV. They are present mainly due to concrete in any building and due to minerals' concentration in a geographical location [28].

For $^{131\text{m}}\text{Xe}$ activity determination in the spectrum of the collection vial, the γ -ray transition of 163.9 keV (1.95% branching) was used. The transition to the ground state proceeds mostly via emission of conversion electrons: 29.8 keV (29.3%), 29.5 keV (15.8%), 33.6–34.5 keV (10.5%), 33.6–33.9 keV (8.5%) [22]. The measurement for Figure 7 was taken in a low-activity environment, free of ^{131}I source. This low background baseline allowed for the precise determination of the radionuclidic purity of $^{131\text{m}}\text{Xe}$ (see Section 3.3).

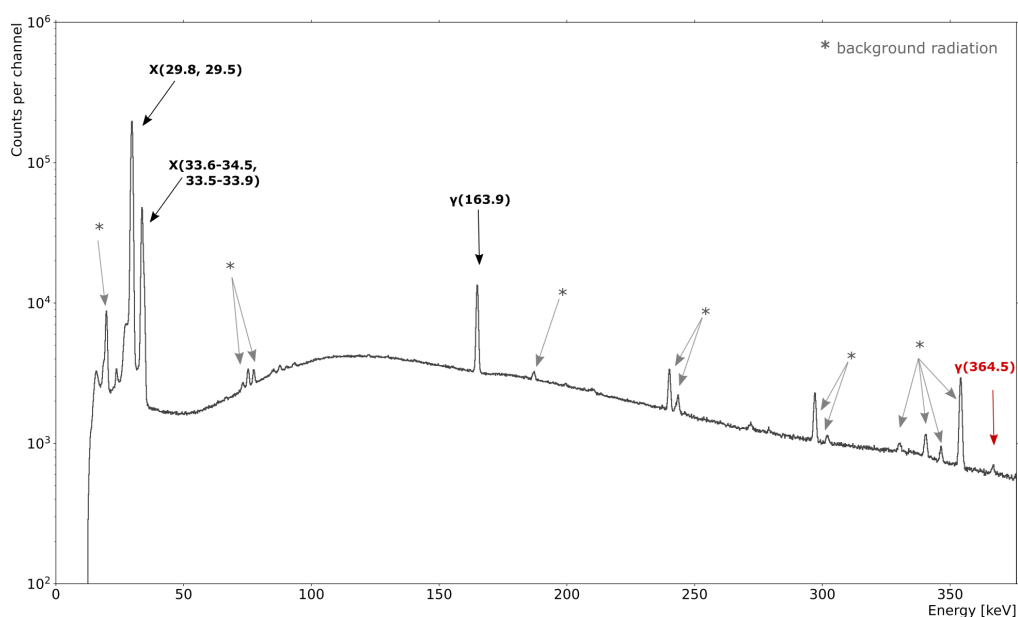


Figure 7. γ -ray spectrum of the collected $^{131\text{m}}\text{Xe}$ sample, recorded in the ISOLDE experimental hall. The decay radiation characteristic of $^{131\text{m}}\text{Xe}$ is labelled in black. The γ -ray transition is at 163.9 keV (1.95%). The X-rays are at: 29.8 keV (29.3%), 29.5 keV (15.8%), 33.6–34.5 keV (10.5%), 33.6–33.9 keV (8.5%). The main γ -ray peak of ^{131}I decay (364.5 keV) is labelled and marked in red. The background γ radiation is marked with grey stars.

Table 2 summarizes the results of experiments with three batches of Na^{131}I and collected $^{131\text{m}}\text{Xe}$.

Table 2. Efficiency of $^{131\text{m}}\text{Xe}$ production and collection from decay of ^{131}I .

ID	Measured ^{131}I Activity at Delivery [MBq] *	Time T between EOM and Delivery [Days]	^{131}I Transfer Rate ρ	Determined $^{131\text{m}}\text{Xe}$ Activity at EOC (Given ρ and α) [kBq]	Measured $^{131\text{m}}\text{Xe}$ Activity at EOC [kBq] *	Efficiency of $^{131\text{m}}\text{Xe}$ Collection
1	49.0(5)	6	64(1)%	119(4)	99(2)	83(3)%
2	51.1(6)	2	85(2)%	149(5)	131(4)	88(3)%
3	47.5(4)	22	96(2)%	240(7)	204(1)	85(3)%

*—measured with Canberra n-type Xtra detector, model GX6020. EOM—end of manufacturing of ^{131}I capsule. EOC—end of collection of $^{131\text{m}}\text{Xe}$. ρ —the transfer rate of ^{131}I from the capsule to the vial. α —the determined release rate of $^{131\text{m}}\text{Xe}$ at ambient conditions.

Column 2 is the measured activity of Na^{131}I capsule in MBq upon delivery of the sample to CERN-ISOLDE. The value for each experiment is in line with the ordered activity (50(5) MBq). Column 3 is the time between the end of manufacturing (EOM) of the Na^{131}I

capsule, reported by Curium Pharma, and the γ -ray spectroscopy of Na¹³¹I capsule at CERN-ISOLDE. It allowed us to determine the initial activity of Na¹³¹I in the capsule, and the production of ^{131m}Xe prior to placing the powder in the experimental setup.

Column 4 (transfer rate ρ) is the percentage of delivered ¹³¹I activity that got transferred to the annealing tube. It was calculated based on two γ -ray spectroscopy measurements: of the ¹³¹I capsule, and of the transferred ¹³¹I powder. The value of ρ varies, as it depends on the Na¹³¹I saturation of the NaI powder and gelatin shell with the ¹³¹I bulk solution during the capsule's preparation process. For instance, for experiment ID 1, a significant percentage of ¹³¹I (about 36%) was in the gelatin shell, which was cast aside.

Columns 5–7 relate to ^{131m}Xe activity. Column 5 details the activity of ^{131m}Xe expected at the end of collection (EOC). The value of ^{131m}Xe activity at the EOC depends on ^{131m}Xe production rate from mother nucleus ¹³¹I, rate of ^{131m}Xe decay and on the losses of ^{131m}Xe due to the room-temperature diffusion out of powder in the time T between EOM and delivery/placement in the experimental system (Column 3). The value in Column 5 was each time calculated in two steps using Equation (1). Firstly, to calculate N_{0mXe} —the number of ^{131m}Xe nuclei produced in Na¹³¹I powder in the time T : $N_{mXe}(T) = N_{0mXe}$. Secondly, to calculate ^{131m}Xe activity at EOC $A_{mXe}(t = t_{EOC})$ (Column 5), using $N_{I_0} = \frac{A_I(0)}{\lambda_I}$, where $A_I(0)$ equals the value in Column 2, and $N_{mXe}(0) = \rho\alpha N_{0mXe}$. α describes the room-temperature diffusion (loss) of ^{131m}Xe from Na¹³¹I powder prior to placement in the experimental setup (in time T). The value α could not be measured directly, because upon delivery the saturation of powder with ^{131m}Xe was unknown (and impossible to measure in situ, due to high ¹³¹I activity). Therefore, the value of α was determined at the end of three experiments as the one providing the best agreement between the calculated and measured activity of collected ^{131m}Xe for all 3 samples (defined by the residuals between calculated and measured values listed in Table 2, Columns 5 and 6). Precisely, we iterated over values of α to find a minimal value of standard deviation function applied to the dataset of efficiency values for all three experiments. The minimum of that function (and the smallest residuals) was obtained for $\alpha = 62\%$. The value $\alpha = 62\%$ was in agreement with the γ -ray spectroscopy measurement of the room-temperature ^{131m}Xe collection—the first collection prior to the series of the high temperature extractions and successive collections. Like other in situ collection measurements, this γ -ray spectroscopy measurement was performed with the n-type SEGe detector, model GC7020 (Canberra).

Column 6 presents the measured ^{131m}Xe activity at EOC. The measurements were taken without the iodine background, and after a complete cycle of heat treatments (see Figure 7). Finally, Column 7 specifies the collection efficiency as a ratio between the measured ^{131m}Xe (Column 6) and the determined ^{131m}Xe activity at EOC (Column 5). The collection efficiency was 85% on average.

3.2. Collection Efficiency as a Function of Temperature

One of the objectives of this work was to establish the most suitable conditions to extract ^{131m}Xe from a Na¹³¹I salt and, as a result, to minimize the workload and time needed to achieve an optimized collection. For this purpose, the collection efficiency as a function of the heating temperature was studied. ¹³¹I was heated up to 400 °C in several steps. The measurements of sample no. 1 were done in a more conservative range of temperatures (up to 300 °C) than for the consecutive samples (up to 400 °C).

Samples 1 and 2 were heated multiple times to temperatures between 40 °C and 100 °C over a course of 14 days. For sample 3, the experiment's protocol was improved and all collections were executed successively on day 14 with each temperature threshold reached only once. Since the setup was not evacuated in between collections, we were not concerned with the loss of xenon outside the measurement system (parameter α) during the experiment.

Figure 8 presents—for each Na¹³¹I sample and as a function of the extraction temperature (x -axis)—the cumulative percentages of ^{131m}Xe extracted up until a given temperature T_c with respect to the total collected activity of ^{131m}Xe (y -axis). For samples 1 and 2, the value at each point in the plot is the sum of the multiple activity increments (with the

activity value adapted using the decay law) contributing to the collection up to a given temperature, divided by the measured end-product ^{131m}Xe activity and expressed as a percentage. For sample 3, it is the cumulative activity of ^{131m}Xe obtained from single collections up to a given temperature, divided by the measured activity of ^{131m}Xe end-product and expressed as a percentage.

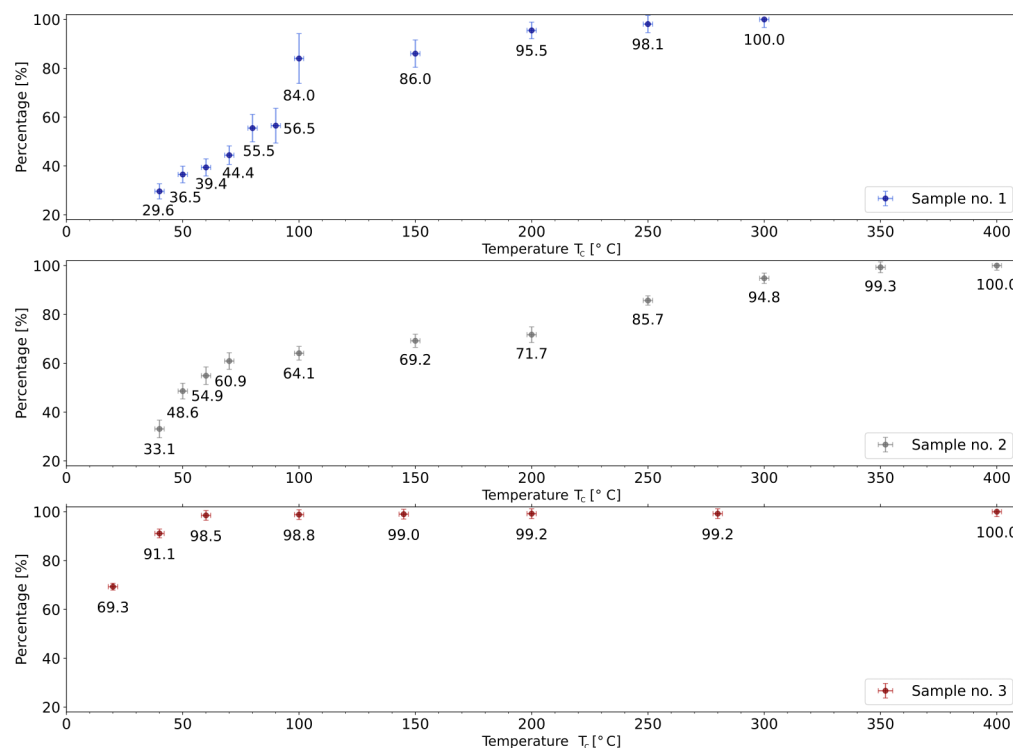


Figure 8. Percentage of ^{131m}Xe activity collected up until temperature T_c normalized to the total collected ^{131m}Xe activity.

For practical reasons, the sample was not replaced between heating cycles at different temperatures. Therefore, the thermal diffusion coefficient could not be derived. However, the collected data allowed to establish that the temperature threshold for ^{131m}Xe diffusion out of Na^{131}I powder is below or at room temperature. For heat treatments up to 100 °C: 84%, 64%, and 99% of all collected ^{131m}Xe was measured for samples 1–3, respectively. In addition, in the first collection—at room temperature—for sample 3, 69% of total collected ^{131m}Xe activity was measured. Consequently, for a time-saving ^{131m}Xe collection operation with relatively minimal losses it would be sufficient to heat the Na^{131}I sample to 200 °C.

3.3. Radionuclidic Purity of Generated ^{131m}Xe

Before utilizing the collected ^{131m}Xe it has to be assured that the potential residues of ^{131}I , i.e., the “breakthrough” of this sublimation generator, remains below an acceptable value. Internal exposure to ^{131}I comprises of the uptake of ^{131}I by thyroid gland and an increased risk of thyroid disease, including thyroid cancer [29].

A useful quantity to characterise the possible ^{131}I contamination of ^{131m}Xe sample is the minimum detectable activity (MDA), here expressed in Bq, at a specified confidence level. It is usually calculated at the 95% confidence level, which means there is a 95% certainty that the activity above MDA threshold would be detected. Calculations of MDA are based on Currie’s derivation for single measurements [30]. With 95% level of confidence, the simplified formula for 364.5 keV emission from ^{131}I reads as follows [31]:

$$\text{MDA} = \frac{k_1^2 + 2\sqrt{2}k_1 \sigma}{t d_{eff} y} \quad (3)$$

where k_1 is the one-sided confidence factor at 95% confidence ($k_1 = 1.645$), t is the time of acquisition, σ is the standard deviation of the background collected at time t , d_{eff} is the detection efficiency for the γ -ray peak at 364.5 keV, and y is the γ -ray intensity per decay for the γ -ray peak at 364.5 keV.

Table 3 presents, for each of the three experiments sorted by ID in Column 1, the following results: MDA of ^{131}I (Column 2), the ^{131}I activity determined from the area under the peak at 364.5 keV (Column 3), the detected presence or absence of radiation from ^{131}I in the spectrum (Column 4) based on the comparison of Columns 2 and 3, and the ratio of ^{131}I residual activity to $^{131\text{m}}\text{Xe}$ activity, expressed in % (Column 5).

Table 3. Minimum detectable activity of ^{131}I in the $^{131\text{m}}\text{Xe}$ collection sample.

ID	MDA [Bq]	Determined ^{131}I Activity [Bq]	Radiation from ^{131}I	Ratio $^{131}\text{I}:$ $^{131\text{m}}\text{Xe}$
1	28.6	186(50)	Present	0.2%
2	4.1	37(13)	Present	0.03%
3	7.4	56(9)	Present	0.03%

As shown in Table 3, for all experiments the counts in the peak area at 364.5 keV were above the MDA limit. Thus, with 95% confidence, ^{131}I was present in $^{131\text{m}}\text{Xe}$ sample and equal 186(50) Bq, 37(13) Bq and 56(9) Bq, for ID 1, 2 and, 3 respectively. The ratio of ^{131}I activity to $^{131\text{m}}\text{Xe}$ activity for three experiments was: 0.19%, 0.03%, and 0.03%. The elevated ratio for the first experiment might come from the residual activity of iodine that remained in the setup from earlier preparatory experiments.

With respect to chemical purity of the collection, some of the stable excipients initially present in Na^{131}I sample would decompose in the high temperature and would be introduced to the collection vial with the end product. These comprise oxides of carbon (0.8 mmol), phosphorus (0.6 mmol), and sulphur (0.15 mmol). The quantities of stable excipients present after thermal decomposition were determined analytically based on the list—provided by Curium Pharma [25]—of ingredients of the supplied source.

4. Discussion

The purpose of this research was to study the generation of the long-lived excited state $^{131\text{m}}\text{Xe}$ by thermal sublimation, from the decay of a commercially obtained ^{131}I solid-state source.

γ -ray spectroscopy showed that with consecutive heat treatments between 40 °C and 400 °C, up to 88% of the determined produced $^{131\text{m}}\text{Xe}$ can be routinely collected. The remaining $^{131\text{m}}\text{Xe}$ is possibly trapped in the Na^{131}I powder, which starts to sinter at ≈ 200 °C. This hypothesis could not be verified with γ -ray spectroscopy because of the high background from the Na^{131}I . In addition, up to 69% of the total $^{131\text{m}}\text{Xe}$ can already be collected at room temperature.

The presented sublimation generator represents a possible way to obtain low activity batches of $^{131\text{m}}\text{Xe}$ with high radionuclidic purity throughout the year, using the well-established distribution network of ^{131}I capsules. The analysis of radionuclidic purity shows that in the end-product vial with $^{131\text{m}}\text{Xe}$, the ratio of ^{131}I residual activity to collected $^{131\text{m}}\text{Xe}$ activity was 0.03% for two samples and 0.19% for one sample—from the first experiment that was possibly contaminated by the earlier preparatory experiments. The generally accepted activity range employed for the inhalation of another xenon gas agent— ^{133}Xe —by an average patient (70 kg) is 74–1110 MBq for the pulmonary function imaging and 370–1110 MBq for cerebral blood flow imaging [32–34]. Tolerable residual level of ^{131}I present in the gas cylinder with ^{133}Xe radiopharmaceutical is 0.01% of total activity present in the sample [32–34], thus the maximum value would be 111 kBq. The necessary $^{131\text{m}}\text{Xe}$ activity in GAMMA-MRI project is: 50–100 MBq and 10–30 MBq, respectively for the polarization optimization and for proof-of-principle experiments in a preclinical MRI device built within the GAMMA-MRI project [35]. Given the experimentally derived ratio ^{131}I to $^{131\text{m}}\text{Xe}$ equal to 0.03% (see Table 3), the residual activity of ^{131}I would be at maximum 30 kBq for the polarization optimization and 9 kBq for proof-of-principle experiments in a preclinical MRI device. In the scope of

next experiments taking place in Switzerland, an additional consideration is to follow the authorization limits (LA) listed in the Swiss Radiological Protection Ordinance [36], which are: 9 GBq for ^{131m}Xe and 0.5 MBq for ^{131}I .

However, despite high radionuclidic purity, some of the stable excipients added to samples are present in the collection vial with the end product. Thus, purification methods of the end product might have to be implemented prior to deployment for the GAMMA-MRI project. A practical limitation is that collection of ^{131m}Xe would have to be planned 13–15 days in advance of a subsequent experiment to allow for ^{131}I decay and production of sufficient amounts of ^{131m}Xe . Thus, an experimental setup needs to be dedicated solely to this goal for a whole period of approximately two weeks.

Finally, several fundamental limitations of the detailed method have to be kept in mind that de facto preclude a significant upscaling of this method. First, the maximum recovered activity of ^{131m}Xe is about 300 times smaller than the ^{131}I activity of the generator, even assuming lossless transfer of Na^{131}I powder to the experimental setup. Further, one has to consider that the ^{131}I mother has fivefold higher γ -ray dose rate per Bq than the ^{131m}Xe daughter, and several orders of magnitude higher radiotoxicity per Bq than ^{131m}Xe . Consequently, upscaling this method to large-scale generators without process automation is undesirable from ALARA considerations, and could run into licensing issues.

5. Conclusions and Outlook

An affordable and accessible production method of small activities of the long-lived ^{131m}Xe isomer via radioactive decay of commercially available ^{131}I was investigated. Our thermal sublimation generator is dedicated to supplying the long-lived ^{131m}Xe for optimization tests of laser polarization in the GAMMA-MRI project. Once larger activity batches of ^{131m}Xe are required for a regular clinical use, the preferred option would be a centralized production in dedicated facilities with centralized quality control. ^{131m}Xe can also be produced by thermal neutron capture on enriched ^{130}Xe samples and the activities and radionuclidic purity achievable in reactor irradiations will be discussed in a forthcoming article [37].

Author Contributions: Conceptualization: R.B.J., M.K., U.K., K.K.; methodology: K.K.; software: K.K., R.L., S.G.P.; validation: M.K., U.K., K.K., R.L., S.G.P.; formal analysis: K.K., R.L., S.G.P.; investigation: M.J.C., K.K., R.L., S.G.P.; resources: N.A., M.B., M.K., K.K., R.L., S.G.P.; data curation: K.K., R.L., S.G.P.; writing—original draft preparation: K.K.; writing—review and editing: R.B.J., M.K., U.K., K.K., R.L., S.G.P.; visualization: K.K.; supervision: R.B.J., M.K.; project administration: R.B.J., M.K.; funding acquisition: R.B.J., M.K. All authors have read and agreed to the published version of the manuscript.

Funding: The GAMMA-MRI project has received funding from the European Union’s Horizon 2020 research and innovation programme under grant agreement No. 964644 (GAMMA-MRI). The authors also wish to acknowledge support via the Swiss Excellence Government Scholarship, the CERN Medical Application Fund (GAMMA-MRI), and the Romanian IFA grant CERN/ISOLDE.

Institutional Review Board Statement: Not applicable.

Informed Consent Statement: Not applicable.

Data Availability Statement: Data supporting the reported results can be found at: <https://cernbox.cern.ch/index.php/s/Eo9CTu5LOo5bx8O> (accessed on 20 September 2022). The detailed study is available on request from the corresponding author.

Acknowledgments: We thank B. Karg, S. Warren, and members of SY-STI-RBS, in particular B. Crepieux, E. Barbero, J. Ballof, and S. Rothe, for discussions, assistance in designing the initial prototype and manufactured parts of the setup, M. Wuillemin for his input on iodine production, J.A. Ferreira Somoza for discussion on Xe cryogenic trapping, J. Schell for assistance in scheduling the experiments. We thank A. Dorsival, E. Aubert, P. Bertreix, N. Menea, A.L. Boscher, and other members of HSE-RP for their support during project execution.

Conflicts of Interest: The authors declare no conflict of interest.

References

1. Oros, A.M.; Shah, N.J. Hyperpolarized xenon in NMR and MRI. *Phys. Med. Biol.* **2004**, *49*, R105. [[CrossRef](#)] [[CrossRef](#)] [[PubMed](#)]
2. Crişan, G.; Moldovean-Cioroianu, N.S.; Timaru, D.G.; Andrieş, G.; Căinap, C.; Chiş, V. Radiopharmaceuticals for PET and SPECT Imaging: A Literature Review over the Last Decade. *Int. J. Mol. Sci.* **2022**, *23*, 5023. [[CrossRef](#)] [[CrossRef](#)] [[PubMed](#)]
3. Zheng, Y.; Zhou, Z. SPECT and PET in Vascular Dementia. In *PET and SPECT in Neurology*; Springer International Publishing: New York, NY, USA, 2021; pp. 563–575. [[CrossRef](#)]
4. Wisser, D.; Hartmann, M. ^{129}Xe NMR on Porous Materials: Basic Principles and Recent Applications. *Adv. Mater. Interfaces* **2021**, *8*, 2001266. [[CrossRef](#)] [[CrossRef](#)]
5. Boventi, M.; Mauri, M.; Simonutti, R. ^{129}Xe Xe: A Wide-Ranging NMR Probe for Multiscale Structures. *Appl. Sci.* **2022**, *12*, 3152. [[CrossRef](#)] [[CrossRef](#)]
6. Walker, T.G.; Happer, W. Spin-exchange optical pumping of noble-gas nuclei. *Rev. Mod. Phys.* **1997**, *69*, 629–642. [[CrossRef](#)] [[CrossRef](#)]
7. Rao, M.R.; Norquay, G.; Stewart, N.J.; Wild, J.M. Measuring ^{129}Xe transfer across the blood-brain barrier using MR spectroscopy. *Magn. Reson. Med.* **2021**, *85*, 2939. [[CrossRef](#)] [[CrossRef](#)] [[PubMed](#)]
8. Berthault, P.; Boutin, C. Biosensing and study of biological cells using hyperpolarized ^{129}Xe . In *Hyperpolarized Xenon-129 Magnetic Resonance: Concepts, Production, Techniques and Applications*; The Royal Society of Chemistry: London, UK, 2015; pp. 261–271. [[CrossRef](#)]
9. Stupic, K.F.; Cleveland, Z.I.; Pavlovskaya, G.E.; Meersmann, T. Hyperpolarized ^{131}Xe NMR spectroscopy. *J. Magn. Reson.* **2011**, *208*, 58–69. [[CrossRef](#)] [[CrossRef](#)] [[PubMed](#)]
10. Kimura, A.; Imai, H.; Fujiwara, H. Continuous flow and dissolved phase ^{129}Xe NMR/MRI for quantification in preclinical study as well as materials science. In *Hyperpolarized Xenon-129 Magnetic Resonance: Concepts, Production, Techniques and Applications*; The Royal Society of Chemistry: London, UK, 2015; pp. 301–316. [[CrossRef](#)]
11. Wang, L.Q. Hyperpolarized ^{129}Xe NMR in materials sciences: Pore structure, interconnectivity and functionality. In *Hyperpolarized Xenon-129 Magnetic Resonance: Concepts, Production, Techniques and Applications*; The Royal Society of Chemistry: London, UK, 2015; pp. 142–163. [[CrossRef](#)]
12. Yokoe, K.; Satoh, K.; Yamamoto, Y.; Nishiyama, Y.; Asakura, H.; Haba, R.; Ohkawa, M. Usefulness of $^{99\text{m}}\text{Tc}$ -Technegas and ^{133}Xe dynamic SPECT in ventilatory impairment. *Nucl. Med. Commun.* **2006**, *27*, 887–892. [[CrossRef](#)] [[CrossRef](#)] [[PubMed](#)]
13. Ziessman, H.A.; O'Malley, J.P.; Thrall, J.H. (Eds.) Chapter 10—Pulmonary System. In *Nuclear Medicine*, 4th ed.; W.B. Saunders: Philadelphia, PA, USA, 2014; pp. 204–226. [[CrossRef](#)]
14. GAMMA-MRI Project Website. Available online: <https://gamma-mri.eu> (accessed on 30 August 2022).
15. *The Supply of Medical Radioisotopes: Interim Report of the OECD/NEA High-Level Group on Security of Supply of Medical Radioisotopes*; Technical Report; Organisation for Economic Co-Operation and Development, Nuclear Energy Agency (NEA): Paris, France, 2010.
16. *Manual on Therapeutic Uses of Iodine-131, Practical Radiation Safety Manual No. 6*; Technical Report; International Atomic Energy Agency (IAEA): Vienna, Austria, 1996.
17. *Molybdenum-99 for Medical Imaging*; Technical Report; National Academies of Sciences, Engineering, and Medicine: Washington, DC, USA, 2016. [[CrossRef](#)]
18. Salacz, J. Reprocessing of irradiated ^{235}U for the production of ^{99}Mo , ^{131}I and ^{133}Xe radioisotopes. Fission molybdenum for medical use. In Proceedings of the Technical Committee Meeting Organized by the IAEA, Vienna, Austria, 3–6 November 1987; International Atomic Energy Agency (IAEA): Vienna, Austria, 1989.
19. Bedrossian, P.; Tóth, G.; Zsinka, L. Herstellung von tragerarmem $^{131\text{m}}\text{Xe}$ durch eine Adsorptionsmethode. *Isot. Environ. Health Stud.* **1968**, *4*, 117–118. [[CrossRef](#)] [[CrossRef](#)]
20. McFarland, R. An Improved Generator of $^{131\text{m}}\text{Xe}$. *Int. J. Appl. Radiat. Isot.* **1974**, *25*, 567–568. [[CrossRef](#)]
21. Zheng, Y.; Miller, G.W.; Tobias, W.A.; Cates, G.D. A method for imaging and spectroscopy using γ -rays and magnetic resonance. *Nature* **2016**, *537*, 652–655. [[CrossRef](#)] [[PubMed](#)]
22. Khazov, Y.; Mitropolsky, I.; Rodionov, A. Nuclear Data Sheets for A = 131. *Nucl. Data Sheets* **2006**, *107*, 2715–2930. [[CrossRef](#)] [[CrossRef](#)]
23. Bateman, H. The solution of a system of differential equations occurring in the theory of radioactive transformations. *Proc. Camb. Philos. Soc.* **1910**, *15*, 423–427.
24. Nahler, G. European Pharmacopoeia (Eur Ph). In *Dictionary of Pharmaceutical Medicine*; Springer: Berlin/Heidelberg, Germany, 2009; p. 69. [[CrossRef](#)]
25. Kulesz, K. (CERN, Geneva, Switzerland); Wuillemin, M. (B.E. Imaging AG, Schwyz, Switzerland). Private communication, 2021.
26. Specification Sheet of DT5730/DT5730S 8 Channel 14 bit 500 MS/s Digitizer from CAEN. Available online: <https://www.caen.it/products/dt5730/> (accessed on 30 August 2022).
27. Livi, R. *MAESTRO Multi-Channel Analyzer Software User's Manual*; AMETEK ORTEC Inc.: Vienna, Austria, 2007.
28. Raeside, D.E.; Brnetich, J. A High-Resolution γ -ray Spectrum of Background Radiation. *Am. J. Phys.* **2005**, *39*, 1396. [[CrossRef](#)] [[CrossRef](#)]
29. Committee on Thyroid Screening Related to I-131 Exposure, Institute of Medicine; Committee on Exposure of the American People to I-131 from the Nevada Atomic Bomb Tests, National Research Council. Health Risks of I-131 Exposure. In *Exposure of the American People to Iodine-131 from Nevada Nuclear-Bomb Tests: Review of the National Cancer Institute Report and Public Health Implications*; National Academies Press: Washington, DC, USA, 1999; Chapter 3, pp. 45–55.

30. Currie, L.A. Limits for Qualitative Detection and Quantitative Determination: Application to Radiochemistry. *Anal. Chem.* **1968**, *40*, 586–593. [CrossRef] [CrossRef]
31. Mirion Technologies (Canberra). Spectrum Analysis Manual. 2017. Available online: <https://www.canberra.com/literature/fundamental-principles/pdf/Spectrum-Analysis.pdf> (accessed on 1 August 2022).
32. Curium US LLC. *Xenon Xe-133 Gas Factsheet*; Curium US LLC: Saint Louis, MO, USA, 2018.
33. Nordion Inc. *Xenon Xe-133 Gas Factsheet*; Nordion Inc.: Ottawa, ON, Canada, 2016.
34. Lantheus Medical Imaging Inc. *Xenon Xe-133 Gas Factsheet*; Lantheus Medical Imaging Inc.: North Billerica, MA, USA, 2018.
35. GAMMA-MRI Collaboration. *Gamma-MRI: The Future of Molecular Imaging*; Grant Agreement ID: 964644; European Commission: Brussels, Belgium, 2021.
36. Le Conseil Fédéral Suisse. *Ordonnance du 26 Avril 2017 sur la Radioprotection (ORaP). Etat le 1er Janvier 2022*; The Swiss Federal Council: Bern, Switzerland, 2022.
37. Kulesz, K.; Chojnacki, M.J.; Köster, U.; Crepieux, B.; Jolivet, R.B.; Korgul, A.; Lica, R.; Michelon, I.; Murawski, L.; Prokopowicz, R.; et al. CERN: Geneva, Switzerland, 2022; (*manuscript in preparation; to be submitted Applied Radiation and Isotopes*).